〈Regular Article〉

Turtle spongious ventricles exhibit more compliant diastolic property and possess larger elastic regions of connectin in comparison to rat compact left ventricles

Takeshi HONDA[1, 2], Yoshihiro UJIHARA[1], Akira HANASHIMA[1], Ken HASHIMOTO[1], Kazuo TANEMOTO[2], Satoshi MOHRI[1]

1) Department of Physiology 1, 2) Department of Cardiovascular Surgery, Kawasaki Medical School

ABSTRACT There is growing evidence that ventricular diastolic dysfunction is a major pathological factor in heart failure. Although many basic and clinical studies have been reported, there is little information available about the comparative and evolutionary aspects of the diastolic properties of vertebrate ventricles. Cardiac tissues in extant vertebrates are roughly divided into two types; compact myocardium in mammals and aves, and spongious myocardium in amphibians and some of reptilians. Here we compared the mechanical properties of both whole ventricles and the biochemical properties of isolated cardiomyocytes (including intracelluar Ca^{2+} ($[Ca^{2+}]_i$) handling, and the lengths of elastic regions of connectin, a protein that determines elasticity of cardiomyocytes) between spongious ventricles of turtles (*Trachemys scripta elegans*) and compact ventricles of Wister rats. Ventricular diastolic function is composed of active relaxation and passive compliance. We investigated ventricular compliance by analyzing normalized end-diastolic pressure-volume relationship (EDPVR) of diastolic-arrested ventricles to compare different-sized hearts and ventricular relaxation by determining logistic time constants of pressure decay. We measured $[Ca^{2+}]_i$ handling using isolated cardiomyocytes. Stiffness constants obtained from exponential curve fitting were significantly larger in rat left ventricles (LVs) compared with turtle ventricles (99.0 ± 7.3 and 2.07 ± 0.62, respectively) showing that rat LVs were much stiffer than turtle ventricles. Normalization of EDPVRs revealed that the turtle ventricle and rat LV exhibit species-specific characteristics in ventricular compliance. At the cellular level, the initial normalized stiffness of rat cardiomyocytes (8.03 ± 1.33 kPa) was 2.8 times higher than in those of the turtle (2.82 ± 0.38 kPa), showing that turtle cardiomyocytes were much more compliant than those of rats. With respect to relaxation, the time constant of isovolumic relaxation in the rat LV pressure-time curve was significantly smaller than that in turtle ventricles (10.7 ± 0.96 and 67.4 ± 3.55 ms, respectively), resulting in early-phase-dominant ventricular filling patterns in rats. The time to peak $[Ca^{2+}]_i$ and the decay time after peak $[Ca^{2+}]_i$ in turtle cardiomyocytes were significantly

Corresponding author
Satoshi Mohri
Department of Physiology 1, Kawasaki Medical School,
577 Matsushima, Kurashiki, 701-0192, Japan
Phone : 81 86 462 1111
Fax : 81 86 462 1121
E-mail: smohri@med.kawasaki-m.ac.jp

longer than in rat. The numbers of amino acids of the PEVK domain of connectin, which is enriched in proline, glutamic acid, valine and lysine and encodes a random coil shown to be an important region in the passive elasticity of connectin were 821 and 204 in turtle and rat ventricles, respectively. These results suggest that vertebrate hearts have been becoming less compliant at the ventricle, cardiomyocyte, and molecular levels during the course of evolution. One possible physiological meaning of restricted compliance in rat ventricles could be related to a well-developed coronary circulation, because the less compliant mechanical properties of the ventricle are largely advantageous to preserve diastolic-dominant coronary arterial flow by preventing excessive ventricular expansion. Future research aimed at understanding the regulatory mechanisms of cardiac connectin among vertebrates may contribute to the investigation of the therapeutic potential of diastolic heart failure.

doi：10.11482/KMJ-E44(1)1 *(Accepted on February 14, 2018)*

Key words：Ventricular mechanics, Diastole, Relaxation, End-diastolic pressure-volume relationship, Myocardial Ca^{2+} handling, Connectin

INTRODUCTION

The heart ejects blood to the lungs and peripheral tissues by repetitive ventricular systolic pumping and diastolic filling, a function that is essential for systemic oxygen supply. Clinically, heart failure is divided into systolic or diastolic dysfunction. The latter has recently been recognized as a major cause of heart failure, and is under intense investigation to characterize the pathophysiology and develop optimal treatments[1-3]. These studies have been performed using mostly rodent models such as mice or rats, and few have investigated the diversity of ventricular mechanics among vertebrates, which may promote better understanding of the regulatory mechanism for cardiac diastolic function.

Diastolic properties are determined by two factors, i.e., ventricular relaxation and compliance[4]. Ventricular relaxation is an active process that decreases ventricular pressure after completion of contraction, which is accomplished intracellularly by exclusion of Ca^{2+} from the cytoplasm of cardiomyocytes via the sarcoplasmic reticulum (SR) Ca^{2+} ATPase (SERCA), and transsarcolemmally by the Na^{+}/Ca^{2+} exchanger (NCX) at the sarcolemma and transverse (T)-tubule membrane. It has been well recognized that prolonging of relaxation occurs during heart failure, along with deterioration of myocardial intracellular Ca^{2+} $[Ca^{2+}]_i$ handling fine structure; for example, the dyadic cleft, where L-type Ca^{2+} channels and the NCX of T-tubules lie in close vicinity to the ryanodine receptors of the SR in mammalian hearts[5]. The time constant of the isovolumic relaxation pressure-time curve is commonly accepted as an index of mechanical ventricular relaxation[6]. On the other hand, ventricular compliance is a passive mechanical property and determined by several factors such as ventricular geometry, the extracellular matrix, and connectin (titin), an elastic molecule generating passive tension during diastole[7].

In vertebrates, there are two kinds of myocardium, compacta and spongiosa, which are associated with the type of cardiac blood supply, i.e., the presence or absence of coronary circulation[8]. Spongious myocardium, which is common in ectothermic animals, possesses wide lacunae to facilitate direct diffusion of oxygen into the tissue. This mesh structure can make spongious myocardium more expandable and result in better ventricular diastolic properties compared with compact myocardium in

homeothermic animals, which receives oxygen from blood via coronary vessels. Despite the obvious morphological differences between vertebrate hearts, the differences (if any) in the diastolic properties of these two types of ventricles have not been investigated.

Although it has been reported that the end-diastolic pressure-volume relationship (EDPVR) is important in the characterization of ventricular compliance[9–11], heart size-independent analysis should be adopted to compare ventricular compliance across variously sized hearts, because larger hearts exhibit greater expandability when ventricular shapes remain the same (Fig. 1A, B). Therefore, we normalized EDPVR by dividing ventricular end-diastolic volume by ventricular wall weight (Fig. 1C). This method is commonly used for normalizing end-systolic pressure-volume relationships (ESPVR), and represents ventricular contraction based on a time-varying elastance

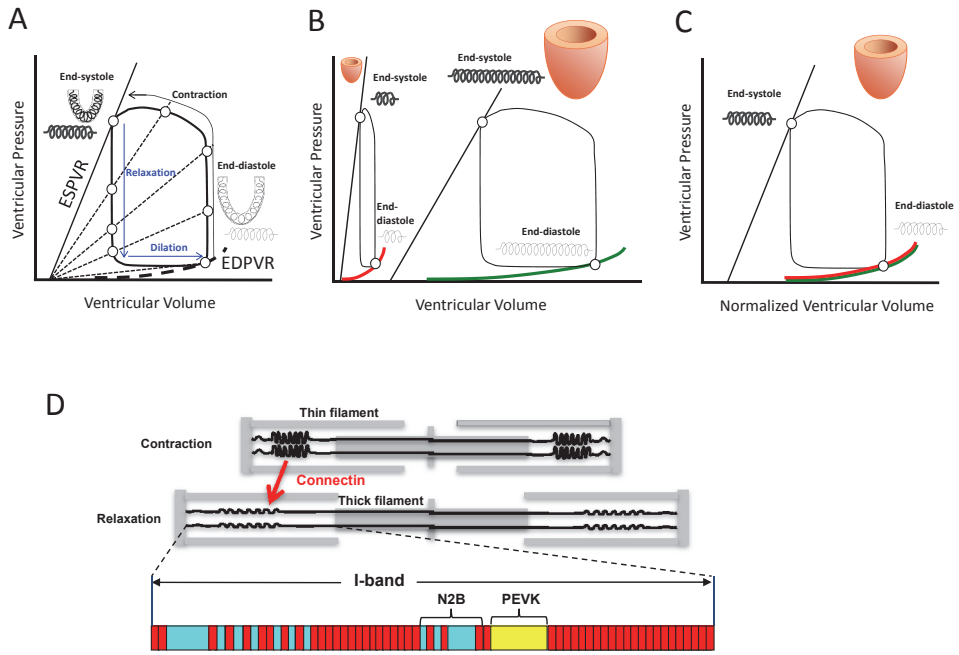

Fig. 1 Schematic illustrations of the time-varying elastance model and the molecular structure of cardiac connectin.
(A) Ventricular systolic activity (contraction) and diastolic activity (relaxation and dilation) are represented as the increase and the decrease of the slope of ventricular pressure-volume relationship with time. The increase and decrease in ventricular elastance are expressed as a thickened spring during contraction and a thinned spring during relaxation and dilation, respectively. ESPVR: end-systolic pressure-volume relationship, EDPVR: end-diastolic pressure-volume relationship.
(B) Schematic drawings of pressure-volume relationships of small and large ventricles, and corresponding conceptual springs in end-systole and end-diastole. The thickness of the spring represents its elastance. Smaller ventricles can be interpreted as shorter springs, and tend to show stiffer diastolic mechanical properties compared with larger ventricles. The same thickness of the spring at end-diastole indicates the same diastolic property per unit of myocardium.
(C) For quantitative analysis of diastolic mechanical properties, EDPVRs of different-sized hearts must be normalized by ventricular weight. The schematic drawing shows that two different-sized hearts (B) show the same EDPVR by dividing end-systolic volume by ventricular wall weight.
(D) The location of connectin during contraction (top) and relaxation (middle). Passive tension produced via connectin during relaxation is regulated by elasticity of expandable regions. Cardiac connectin isoforms include constitutive Ig domains (red), unique sequences (blue) and PEVK domains (yellow; rich in proline [P], glutamate [E], valine [V], and lysine [K]) in the I-band (bottom). N2B and PEVK domains possess elasticity and work as springs in cardiomyocytes.

model [11, 12] (Fig. 1A).

In addition to whole ventricle analysis, cellular and molecular studies are useful for a better understanding of the mechanisms by which diastolic properties are regulated. Therefore, we investigated the mechanical properties of isolated cardiomyocytes and determined the primary structure of the protein connectin (also called titin). Connectin is striated muscle-specific and the largest protein that connects Z-line to the M-line in half-sarcomeres (Fig. 1D). It is a very large protein with a molecular mass of 3-4 MDa, and functions to maintain sarcomere length and to determine expandability of cardiomyocytes in the heart. In particular, the PEVK domain of connectin, which is rich in proline, glutamate, valine and lysine, functions as an elastic coil, and therefore longer PEVK domains produce more expandable cardiomyocytes and compliant ventricles (Fig. 1D). In addition, we also compared the lengths of the other elastic connectin region (N2B).

The purpose of this study was to compare the diastolic properties of turtle (*Trachemys scripta elegans*) ventricle, which consists of a thick inner avascular spongious myocardium and a thin outer compact layer, with Wister rat left ventricle (LV), which fully consists of compact myocardium. To this end, we investigated: ventricular compliance (by analyzing normalized EDPVR); stiffness of isolated cardiomyocytes; ventricular relaxation (by determining logistic time constants of ventricular pressure decay); $[Ca^{2+}]_i$ handling by isolated cardiomyocytes; and the primary structure of the elastic regions of connectin.

MATERIALS AND METHODS

Surgical preparation

Experiments were performed on 8-week-old male Wister rats (weighing 240-260 g) and turtles (T. s. elegans, weighing 1.10-1.55 kg). Rats were anesthetized with sevoflurane (2-5%) and intubated. They were mechanically ventilated using a volume-controlled ventilator (SN-480-7 Shinano, Japan) with tidal volume 2 ml and respiratory rate 90 breaths/min. Bilateral sternotomy was performed, and left atrium (LA) and LV pressures were simultaneously recorded by a fluid-filled 18-gage needle for pressure decay analysis. The heart was then rapidly excised and perfused with cardioplegic solution (Na^+: 120.0 mEq/L, K^+: 16.0 mEq/L, Mg^{2+}: 32.0 mEq/L, Ca^{2+}: 2.4 mEq/L, HCO_3^-: 10.0 mEq/L, Cl^-: 160.4 mEq/L; Miotector®, Mochida, Japan) by Langendorff perfusion, resulting in diastolic arrest. A thin latex balloon attached to an end of a stiff polyethylene tube was fitted into the LV of the isolated heart. The balloon and tube were filled with water and connected to a fluid-filled pressure transducer and micro-syringe that controlled LV volume. LV volume was increased until LV pressure reached 20 mmHg.

Turtles were anesthetized with an intramuscular injection of 3-aminobenzoic acid ethyl ester methanesulfonate (0.5 g/kg body weight). After removal of the turtle's plastron, pressures of LA and ventricle were simultaneously recorded in the same fashion as rats for pressure decay analysis. The heart was then excised and submerged in the same cardoplegic solution to stop beating and remove blood. Atriums, pulmonary artery and aorta were ligated and polyethylene tube was inserted from an apical incision and connected to the pressure transducer and syringe to measure pressure and volume simultaneously. Ventricular volume was increased until ventricular pressure reached 20 mmHg. All animal procedures were approved by the Institutional Animal Care and Use Committee at the Kawasaki Medical School, which is based on the National Institutes of Health Guide for the Care and Use of Laboratory Animals.

Analysis of EDPVR and time constant of pressure decay

EDPVRs were constructed and fit to the

exponential equation

$$P = a \cdot e^{EDV \cdot b} + c$$

where b is an index of ventricular stiffness, c is the intercept along the pressure axis, and EDV is end-diastolic volume[9, 10]. Ventricular relaxation was evaluated by determining minimum rate of pressure change (-max dP/dt) and the time constant of pressure decay during relaxation, as indexed by the logistic time constant. A logistic model for LVP(t) during relaxation was given by

$$P(t) = \alpha / [\, 1 + \exp (t/_{\tau L}) \,] + \beta ,$$

where α is an amplitude constant, β is a nonzero asymptote, t is time, and $_{\tau L}$ is the time constant of the exponent[6]. For calculation of $_{\tau L}$, we analyzed the time constant of isovolumic relaxation from the time of peak -dP/dt to the time when LVP fell to 5 mmHg above the EDP using a least-squares method. These analyses were performed in Kaleida Graph (Synergy software, USA).

Cardiomyocyte preparation

Turtles were anesthetized with an intramuscular injection of overdose of 3-Aminobenzoic Acid Ethyl Ester Methanesulfonate. The plastron was quickly removed and the heart was excised. A cannula was inserted into the right aortic arch for retrograde perfusion with 10 ml cell isolation buffer (CIB) containing 0.4 mM EGTA (EGTA-CIB). The CIB was composed of (mM unless stated): 130 NaCl, 5.4 KCl, 0.5 $MgCl_2$, 0.33 NaH_2PO_4, 22 glucose, 25 HEPES-NaOH (pH=7.4) and 50 μU/ml bovine insulin (Sigma-Aldrich, USA). After washing out blood, the ventricle was cut into several pieces and washed three times with 10 ml EGTA-CIB for 3 min by gentle agitation. The tissue pieces were digested twice with 0.3 mM $CaCl_2$, 1 mg/ml collagenase type II (Worthington Biochemical Corp., USA), 1 mg/ml protease (Sigma-Aldrich, USA) in CIB for 20 min at 37℃ with gentle agitation. After the cell suspension was centrifuged at 14 × g for 5 min, the pellet was resuspended in CIB supplemented with 1.2 mM $CaCl_2$ and 2 mg/ml bovine serum albumin (BSA) (Sigma-Aldrich, USA). After cells were incubated for 10 min at room temperature (20℃), the cell suspension was centrifuged at 14 × g for 5 min, and resuspended in Tyrode's solution supplemented with 2 mg/ml BSA. The Tyrode's solution was composed of (mM): 140 NaCl, 5.4 KCl, 1.8 $CaCl_2$, 0.5 $MgCl_2$, 0.33 NaH_2PO_4, 11 glucose and 5 HEPES-NaOH (pH = 7.4).

Rat ventricular cardiomyocytes were obtained by an adaptation of isolation protocols previously described for mice[5, 13]. Briefly, the heart was excised and a cannula was inserted into the aorta. Coronary perfusion was initiated with EGTA-CIB. After 5 min, the perfusate was then changed to the enzyme solution with 0.3 mM $CaCl_2$ for 10 min. The enzyme solution consisted of CIB with 0.3 mM $CaCl_2$, 1 mg/ml collagenase type II, 0.06 mg/ml protease and 0.06 mg/ml trypsin (Sigma-Aldrich). The left ventricles were minced and further digested in the enzyme solution with an additional 0.7 mM $CaCl_2$ and 2 mg/ml BSA for 20 min with gentle agitation. After centrifugation at 14 × g for 5 min, the pellet was resuspended in CIB supplemented with 1.2 mM $CaCl_2$ and 2 mg/ml BSA, and then incubated for 10 min at 37℃. After repeat centrifugation, cells were resuspended in Tyrode's solution supplemented with 2 mg/ml BSA.

Cell shortening/relengthening and morphology measurements

To measure cell shortening, isolated cardiomyocytes were stimulated in an electrical field at 0.2 Hz using a two-platinum electrode insert connected to an isolator (SS-104J, Nihon Kohden, Japan) and a bipolar stimulator (SEN-3401, Nihon Kohden) on the stage of an inverted microscope (IX73, Olympus, Japan) with a 20× objective lens (UCplanFLN, Olympus). Cell shortening was recorded using the first sCMOS camera (ORCA flash 4.0, Hamamatsu Photonics, Japan).

Cell shortening/relengthening and morphology were analyzed by MetaMorph software (version 7.8.0.0; Molecular Devices, USA). Because turtle cardiomyocytes have spindle-shaped morphology, the length was measured as length along the midline of the cell, and the width was obtained by dividing projected area by length.

Ca^{2+} transient measurements

Isolated cardiomyocytes were loaded with 5 μM Fura-2 AM (Dojindo, Japan) for 30 min to quantify intracellular Ca^{2+} ($[Ca^{2+}]_i$) as previously described (19). Fura-2-loaded cells were alternately excited at 340 and 380 nm using a DeltaRam spectrofluorophotometer (Photon Technology International, USA) equipped with a cell shortening measurements system. Cells were electrically stimulated and evoked Ca^{2+} transients were evaluated as the fluorescence ratio (excitation at 340 nm/380 nm) using MetaMorph software.

Isolated cell mechanical measurement and analysis

A laboratory-made tensile test system was built in an inverted microscope (IX-73, Olympus) equipped with a 40x water immersion objective lens (UAPON40XW340, Olympus). The isolated cardiomyocyte was held and stretched using two glass microneedles, which differed in stiffness. The flexible needle, whose spring constant was 2.8-89.2 nN/μm, was used for measurement of force applied to the cells by observing its deflection. The needle was attached to a three-axis motorized micromanipulator (EMM2, Narishige, Japan). The rigid needle, whose spring constant was at least two orders of magnitude higher than that of the deflectable needle, was moved to stretch the cell in the major axis direction of the cell by using piezo-actuator (SSL-Z250H, Syouei System Co., Ltd., Japan). The rigid needle and piezo-actuator were moved with three-axis oil hydraulic micromanipulator (MWO-3, Narishige). Before the capture of cells, the tips of microneedles were coated with a biological adhesive, MyoTak™ (Ionoptix, Milton, MA, USA)[14]. Cells were captured by gently pressing down the surface of the cell with needles. The captured cell was then lifted off the chamber bottom and stretched at a rate of 1 μm/s by moving the rigid needle with a piezo-actuator. The experiments were performed at room temperature. Images of the stretching cells were recoded with the first sCMOS camera (ORCA flash 4.0, Hamamatsu Photonics).

After the tensile test, the recorded images were analyzed with Image J 1.51n software (National Institutes of Health, USA). Sarcomere length L was determined by the fast Fourier transform (FFT) as computed by SarcOptiM[15], a plug-in for the Image J. The sarcomere strain ε was defined as $L - L_0$, where L_0 is the initial value of L. The force applied to cell F was calculated by multiplying the deflection of the deflectable needle X with the spring constant k_d, which was determined by cross-calibration method[16, 17]. To remove the effect of cell dimension on tensile properties, normalized force σ was determined as $\sigma = F/A_0$, where A_0 is initial cross-sectional area perpendicular to the stretch direction. The cross section was assumed to be an ellipse whose major axis is the cell width and the minor axis is the cell height[18]. The cell height was estimated by cell width, based on the ratio of cell height to cell width[19]. Tensile properties of the cells were evaluated as force - sarcomere strain (F - ε) and normalized force - sarcomere strain (σ - ε) curves. The initial stiffness S_{ini} and initial normalized stiffness E_{ini} were evaluated as the slopes of the force - sarcomere strain and normalized force - sarcomere strain curves for 0 - 0.05 sarcomere strain ε on the basis of the assumption that the curves were piecewise linear.

RT-PCR

Total RNAs were isolated from ventricles of adult

turtle and rat using TRIzol reagent (Thermo Fisher Scientific) using a previously described procedure[20]. First-strand cDNAs were synthesized with random primers using Superscript-II reverse transcriptase (Invitrogen), following the manufacturer's methods. Primers for amplification of turtle connectin were designed with reference to the exon-intron structure of turtle connectin gene. Primers for amplification of rat connectin were designed with reference to the predicted sequence of N2BA isoform of rat connectin (NCBI accession: XM_017592328.1). Fragments of each parts of connectin were PCR amplified using Phusion polymerase (New England Biolabs). A full length of PEVK fragment on turtle connectin was amplified using PrimeSTAR HS DNA Polymerase (Takara Bio). PCR products were isolated from agarose gel using a GEL/PCR Purification Mini Kit (Favorgen) and sequenced (FASMAC Co., Ltd.).

Immunofluorescence microscopy

Immunostaining of turtle and rat heart was performed as described previously[5, 13]. Excised hearts were embedded in OCT compound (Tissue-Tek) and frozen. Frozen tissues were cut into 7-μm-thick sections. These sections were air-dried and then washed with phosphate-buffered saline (PBS). After the sections were permeabilized with 0.1% Triton X-100 for 5 min, they were incubated in blocking solution for 1 h. Subsequently, the sections were incubated with polyclonal antibodies for the N-terminus of chicken connectin (PcCOM1)[21] or the C-terminus of chicken connectin (Pc72C)[22] and monoclonal α-actinin antibody (A7811, Sigma) as the primary antibodies for 1 h at 4℃. After the sections had been washed with PBS containing 0.1% Tween 20 (PBS-T), they were exposed to Alexa Fluor 488-conjugated anti-rabbit IgG (A11008, Life Technologies) and Alexa Fluor 568-conjugated anti-mouse IgG (A11001, Life Technologies) as secondary antibody for 15 min at 4℃. The sections were then washed with PBS-T again and mounted with Dako fluorescent mounting medium (Dako). Fluorescent images were obtained using a confocal laser scanning microscope (FV1000, Olympus) with a UPlanApo ×60/1.35 oil immersion objective lens (Olympus).

SDS-Agarose electrophoresis

Connectin proteins were analyzed as previously described[23]. Briefly, muscle tissues were homogenized using a Kinematica™ Polytron™ homogenizer (PT1600E; Fisher Scientific, MA, USA) in a sample buffer (8M urea, 2M thiourea, 3% SDS, 75mM DTT, 0.03% bromophenol blue, and 0.05M Tris-HCl pH 6.8 supplemented with Halt™ protease inhibitor cocktail (Thermo-Fisher, MA, USA)). Samples were then heated at 60℃ for 10 min and centrifuged. The supernatant was electrophoresed on 1% vertical agarose gels (30% glycerol, 0.05M Tris base, 0.384M glycine, and 0.1% SDS) at 10mA for ~2h. The composition of the lower electrophoresis buffer was 0.05M Tris base, 0.384M glycine, and 0.1% SDS. The upper buffer contained the same with the addition of 10mM β-mercaptoethanol. Proteins were visualized with Coomassie brilliant blue (Bio-Safe CBB G-250, Bio-Rad, CA, USA). Gels were then imaged with the calibrated imaging densitometer (GS-800, Bio-Rad), and connectin proteins were identified.

RESULTS

EDPVR analysis

The average weight of turtle ventricles was 20.0 ± 3.59 g and the average rat LV weight was 7.32 ± 0.448 g. EDPVRs obtained from four rats (of similar age and body weight) and spanning a narrow range are shown in Fig. 2A. In contrast, EDPVRs from four turtles of various weights spanned a relatively wide range (Fig. 2B). The values of *b* representing ventricular stiffness in turtles and rats were 1.02 ± 0.22 and 93.0 ± 22.7 respectively, indicating

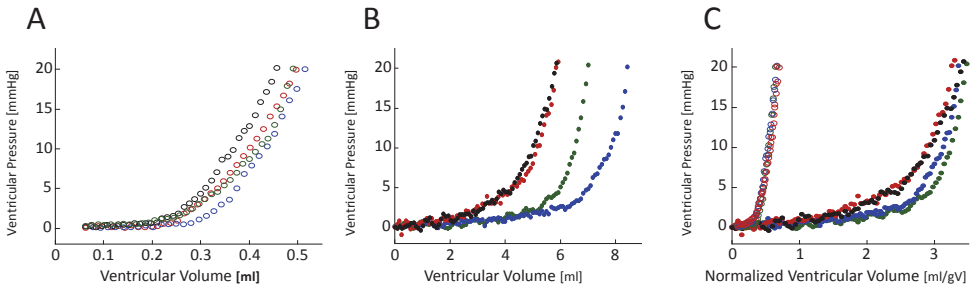

Fig. 2 Diastolic property via ventricular pressure-volume relationship of rat left ventricles and turtle ventricles.
(A) EDPVRs obtained from four rat ventricles. Colors of open circles represent each animal.
(B) EDPVRs obtained from four turtle ventricles. Colors of closed circles represent each animal.
(C) Normalized EDPVRs of corresponding rat and turtle ventricles.

Table 1. Variables of ventricular diastolic functions

Variable	Turtle (n = 4)	Rat (n = 4)
b (EDPVR)	1.02 ± 0.22	93.0 ± 22.7*
b (nEDPVR)	2.07 ± 0.62	99 ± 7.3*
Ventricular weight ($x10^{-1}g$)	20.0 ± 3.59	7.32 ± 0.448*
V_{P20} (ml)	6.80 ± 1.20	0.490 ± 0.023*
nV_{P20} ($ml \cdot gV^{-1}$)	3.14 ± 0.54	0.674 ± 0.154*
τ_L (ms)	67.4 ± 3.55	10.7 ± 0.96*
-max dP/dt ($mmHg \cdot s^{-1}$)	171.4 ± 56.9	3,407 ± 350*

Each value indicates mean ± SD. b, stiffness constant; nEDPVR, normalized end-diastolic pressure-volume relationship; V_{P20}, normalized volume at which pressure reached 20 mmHg; n-EDV, EDV normalized for 1 g LV weight; -max dP/dt, maximum negative value of time derivative of LV pressure; τ_L, time constant of isovolumic relaxation pressure segment after -max dP/dt. Statistically significant difference at *: $p < 0.05$ compared to turtle.

that the ventricles of turtles are significantly more complaint than those of rats (Table 1). Normalization of EDPVRs by ventricular weight revealed that turtle ventricles and rat LVs show species-specific characteristics in ventricular compliance (Fig. 2C, Table 1). The normalized ventricular volume at which ventricular pressure reached 20 mmHg (nV_{P20}) in turtles was approximately four times greater than that in rats, and the values spanned a narrow range in each species (Table 1).

Simultaneous pressure measurement in atrium and ventricle

Fig. 3 (A, B) shows representative simultaneous tracings of LA and ventricular pressures in turtle, and of LA and LV pressures in rat, respectively. During diastole, LA pressure was higher than ventricular or LV pressure as shown in Fig. 3C. The time courses of pressure gradients in turtle atria and ventricles exhibited late-phase dominance. In contrast, rat hearts exhibited early-phase dominant pressure gradient patterns. Moreover, LV pressure in rats, but not in turtles, dropped below zero. With regard to ventricular relaxation, Fig. 3D shows a representative set of logistic curves (black dashed lines) best-fitted to ventricular relaxation pressure curves (open red circles: rat, closed red circles: turtle). Anatomically, atriums of turtle were much

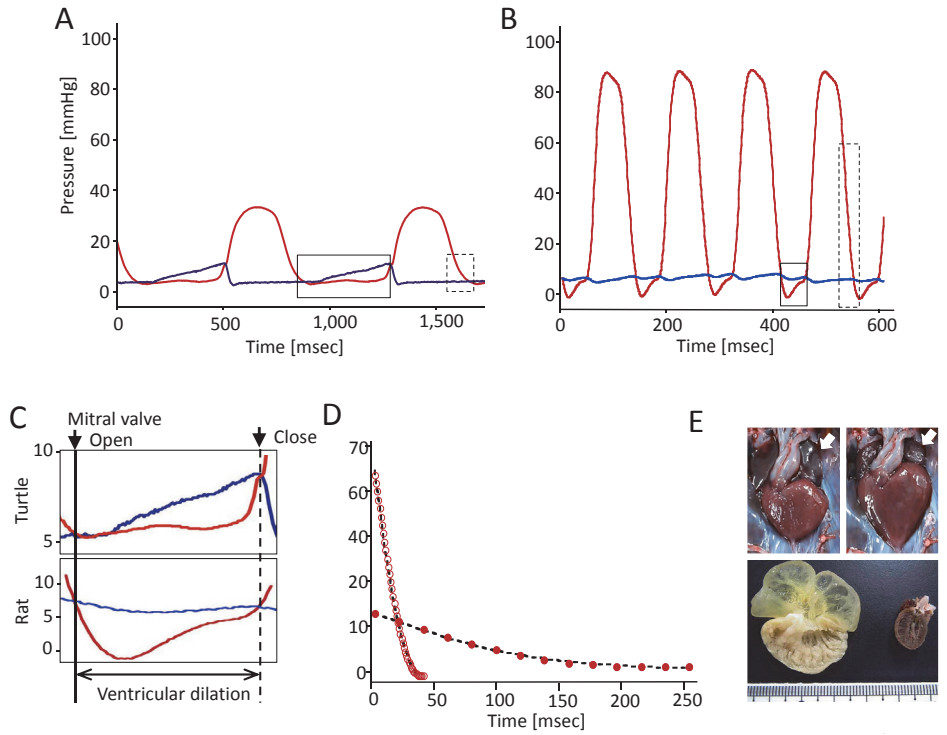

Fig. 3 Ventricular and atrial hemodynamics.
(A) Simultaneous recording of ventricular (red) and left atrial (blue) pressures in turtles. Solid and dashed squares are magnified in (C) and (D), respectively.
(B) Simultaneous recording of left ventricular (red) and left atrial (blue) pressures in rats. Solid and dashed squares are magnified in (C) and (D), respectively.
(C) Representative tracings of ventricular and atrial pressures during ventricular dilation. Timings at which mitral valve opens and closes are shown with solid and dashed line, respectively.
(D) Plots of turtle ventricular (closed red circle) and rat left ventricular (open red circle) pressures. X-axis shows ventricular pressure falling from the points of the time of peak -dP/dt.
(E) Macroscopic appearance of the turtle and rat hearts. Systolic (upper left panel) and diastolic (upper right panel) turtle heart. Lower panel shows the fixed hearts of turtle (left) and rat (right). Arrows indicate left atrium.

larger than those of rats, and ventricle of turtle was filled mostly by atrial contraction during diastole (Fig. 3E). Turtle ventricles exhibited a significantly larger time constant, τ_L, and a lower rate of pressure change (Table 1). According to these hemodynamic analyses, turtle ventricles are characterized by better compliance and slower relaxation when compared to rat LVs.

Morphology and shortening/relengthening properties of isolated cardiomyocytes

To develop a better understanding of the differences in ventricular relaxation in rats and turtles at the single cell level, cellular morphology, shortening, and relengthening of isolated cardiomyocytes were analyzed. Cardiomyocytes isolated from turtles were spindle-shaped, and significantly longer and thinner than those from rat (Fig. 4A-D). The projected area of turtle cardiomyocytes was much smaller than that of rat cardiomyocytes (Fig. 4A, E). Sarcomeres of turtle cardiomyocytes was statistically longer than those of rat (Fig. 4F), and cell shortening was significantly higher in turtle cardiomyocytes than in rat (Fig. 4G,

H). Time to peak and overall duration of contraction were much longer in turtle cells than in rat cells (Fig. 4G, I). The time from peak shortening to 50% relengthening and the time constant of relengthening for turtle cells were also significantly greater than those for rat cells (Fig. 4G, J, K), demonstrating that turtle cardiomyocytes are inferior to rat cardiomyocytes in relaxation ability.

Ca^{2+} measurements in isolated cardiomyocytes

Contraction and relaxation of cardiomyocytes is controlled by $[Ca^{2+}]_i$. In mammalian cardiomyocytes, T-tubule membranes are developed to allow the rapid changes in $[Ca^{2+}]_i$ that facilitate strong and fast heart beats. In contrast, turtle cardiomyocytes do not have a T-tubule system[19]. Consistent with a previous study, the membrane-binding dye di-8-ANEPPS revealed that a striated staining pattern of

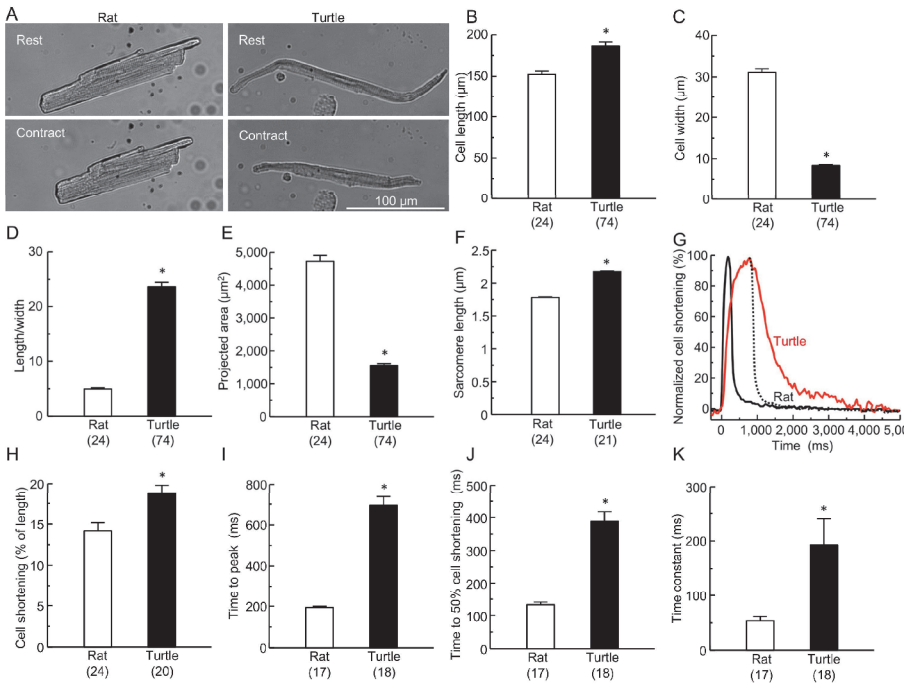

Fig. 4 Morphology and shortening/relengthening of single cardiomyocytes isolated from rats and turtles.
(A) Representative images of rat and turtle cardiomyocytes at rest and during contraction.
(B) Cell length (rat: 152.3 ± 4.0 μm, turtle: 186.1 ± 4.9 μm).
(C) Cell width (rat: 31.0 ± 0.9 μm, turtle: 8.3 ± 0.2 μm). Cell width was calculated by dividing projected area by cell length.
(D) Length/width (rat: 5.0 ± 0.2, turtle: 23.6 ± 0.8).
(E) Projected area (rat: 4,724.5 ± 177.9 μm^2, turtle: 1,551.0 ± 64.8 μm^2).
(F) Sarcomere length at rest (rat: 1.78 ± 0.008 μm, turtle: 2.17 ± 0.011 μm).
(G) Representative traces of normalized cell shortening and relengthening. Dotted line shows normalized cell shortening of rat cardiomyocytes during relengthening. The line is corrected so that the time point of the maximum cell shortening of rat coincides with that of turtle.
(H) Cell shortening (rat: 14.2 ± 0.9%, turtle: 18.8 ± 1.0%).
(I) Time to peak shortening (rat: 193.1 ± 7.7 ms, turtle: 695.0 ± 43.4 ms).
(J) Time from peak shortening to 50% relengthening (rat: 133.1 ± 8.0 ms, turtle: 388.9 ± 28.3 ms).
(K) Relengthening time constant (rat: 53.7 ± 7.8 ms, turtle: 192.9 ± 47.5 ms). Time constant was calculated by fitting a logistic curve to the cell shortening (from maximum relengthening rate to 0% cell shortening).
Values are expressed as means ± SEM. ( ) shows number of cells. Cells were isolated from 3 animals. * $p < 0.05$ vs. rat cardiomyocytes based on unpaired t-test.

T-tubule structures in rat cardiomyocytes, and this was not observed in turtle cardiomyocytes (Fig. 5A). As expected, the time to peak $[Ca^{2+}]_i$ and the decay time after peak $[Ca^{2+}]_i$ in turtle cardiomyocytes were significantly longer than in rat cardiomyocytes (Fig. 5B-E). These results suggest that Ca^{2+} handling in cardiomyocytes correlates with cardiac function in turtles.

Passive tensile property of isolated cardiomyocytes

Next, to compare ventricular compliance at the single cell level, we measured passive tensile property directly along the longitudinal axis of cardiomyocytes isolated from both turtles and rats. Cardiomyocytes isolated from rat and turtle ventricles were stretched ~20% of resting lengths (Fig. 6A). As shown in Fig. 6B, the slopes of the force-sarcomere strain curves of rat cells were much steeper than those of turtle. Initial stiffness was 2.21 ± 0.38 μN and 0.13 ± 0.02 μN for rat and turtle cardiomyocytes, respectively (Fig. 6C). These results demonstrated that the compliance of rat cardiomyocytes was restricted compared to turtle. Rat cardiomyocytes had larger cross-sectional area compared with the turtle cardiomyocytes (Fig. 5), and so, to exclude the effect of cell size, we normalized the stretch force using the cross-sectional area (Fig. 6D). From the normalized force-sarcomere strain relationship obtained, the initial normalized stiffness of rat cardiomyocytes (8.03 ± 1.33 kPa) was 2.8 times higher than that of the turtle (2.82 ± 0.38 kPa) (Fig. 6E). These results suggest

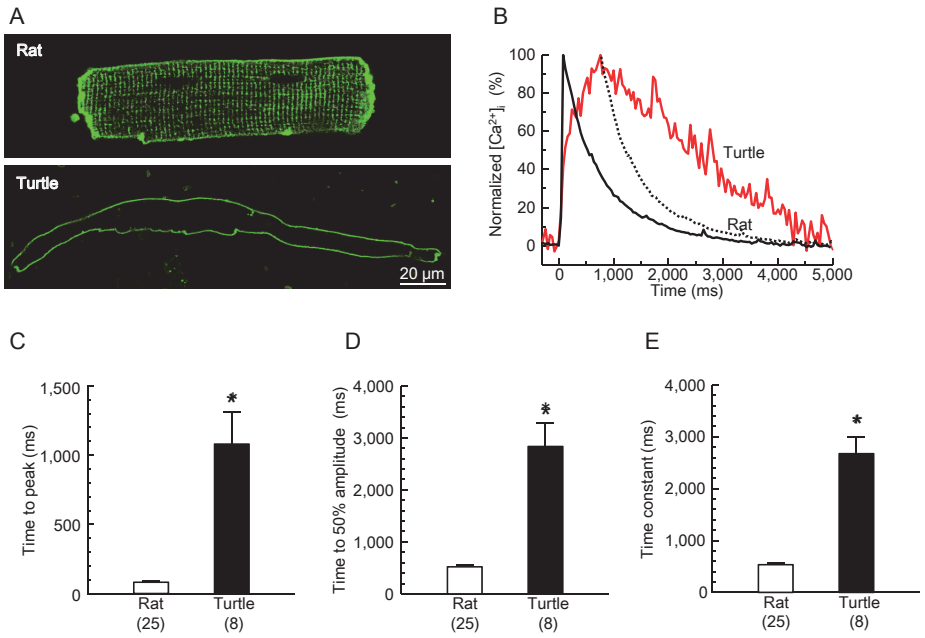

Fig. 5 Ca^{2+} transient in single cardiomyocytes isolated from rats and turtles.
(A) Representative images of rat and turtle cardiomyocytes stained with di-8-ANEPPS.
(B) Representative traces of normalized $[Ca^{2+}]_i$ transients. Dotted line shows normalized $[Ca^{2+}]_i$ transients of rat during Ca^{2+} decay. The line is corrected so that the time point at the peak amplitude of rat coincides with that of turtle.
(C) Time to peak amplitude (rat: 87.3 ± 7.7 ms, turtle: 1,078.8 ± 230.0 ms).
(D) Time from peak amplitude to 50% decay (rat: 520.1 ± 21.3 ms, turtle: 2,832.5 ± 452.8 ms).
(E) Decay time constant (rat: 533.7 ± 37.3 ms, turtle: 2,674.8 ± 321.5 ms). Time constant was calculated by fitting a logistic curve to $[Ca^{2+}]_i$ transient (from maximum decay rate to 0% amplitude).
Values are expressed as means ± SEM. ( ) shows number of cells. Cells were isolated from 3 animals. * $p < 0.05$ vs. rat cardiomyocytes based on unpaired t-test.

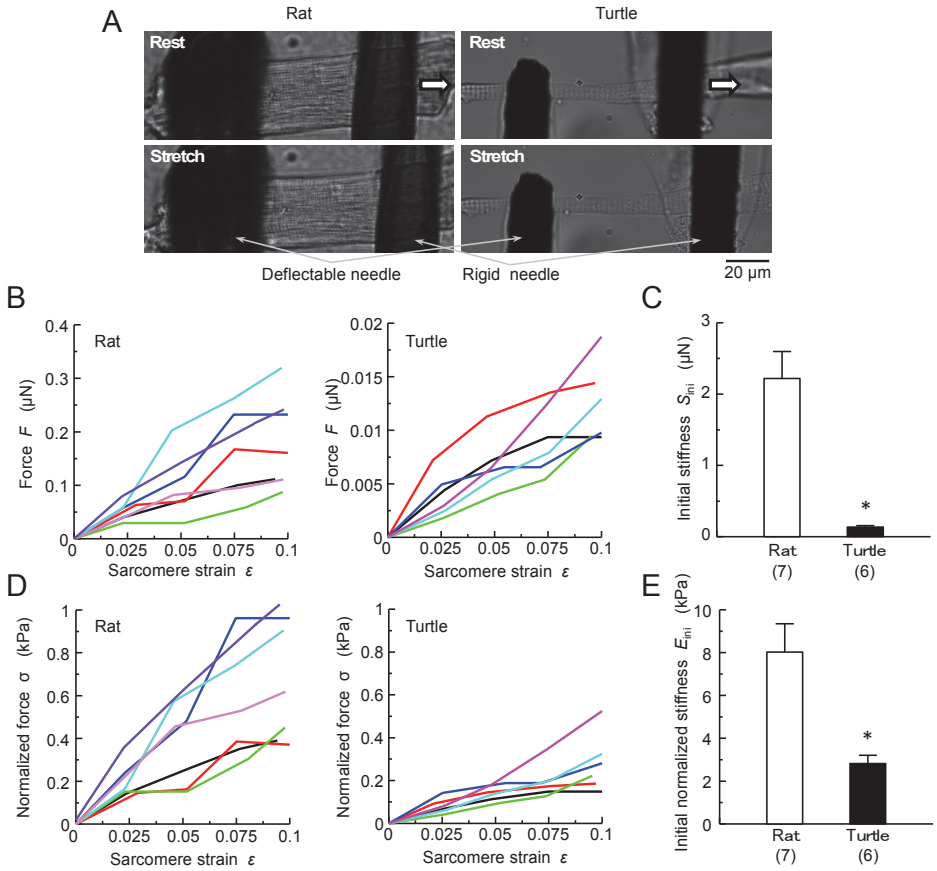

Fig. 6 Tensile tests of single myocytes isolated from rats and turtles.
(A) Typical examples of images of isolated cardiomyocyte during tensile tests.
(B) Force-sarcomere strain curves of isolated cardiomyocytes.
(C) Initial stiffness (rat: 2.21 ± 0.38 μN, turtle: 0.13 ± 0.02 μN).
(D) Normalized force-sarcomere strain curves of isolated cardiomyocytes.
(E) Initial normalized stiffness (rat: 8.03 ± 1.33 kPa, turtle: 2.82 ± 0.38 kPa).

that there is a difference in passive tensile properties between rat and turtle cardiomyocytes at a cellular component level.

Comparison of the elastic region of connectin in turtle heart to rat heart

We stained turtle ventricles with antibodies for the N- or C-terminal region of connectin and Z-line protein α-actinin and observed them by immunofluorescence microscopy to investigate the localization of connectin in turtle ventricles (Fig. 7A). Antibody to the N-terminal region of connectin stained at the Z-line and antibody to the C-terminal region stained at the M-line of the sarcomere in turtle ventricles. These results indicate that the localization of connectin in turtle ventricles is identical to that in rat. SDS-agarose gel electrophoresis showed that the molecular weight of turtle heart connectin was larger than that of rat heart, but smaller than the largest soleus connectin in rat (Fig. 7B). The larger molecular weight of connectin in turtle heart was due to the expression of the N2BA isoform in turtle heart and the N2B isoform in rat heart.

To examine the elasticity of turtle heart connectin, we amplified partial region on turtle connectin by RT-PCR using primers from the adult ventricle of *Trachemys scripta*, which is a turtle that belong to same subfamily to Chrysemys picta. When we compared turtle heart connectin to rat heart connectin, we found that the two units of N2A region are expressed in turtle heart but not in adult rat heart, indicating that connectin in turtle is similar to the N2BA isoform that is expressed in mammalian fetal ventricles (Fig. 7C). Additionally, we found the N2B and PEVK domains, which function to confer extensibility to connectin, were substantially longer in turtle heart connectin than in the rat heart protein. The resting length of turtle heart connectin was calculated to be 0.42 μm longer than that of rat. The difference in lengths between the I-band region of connectin in turtle heart and rat heart corresponded to the difference in sarcomere lengths between in turtle heart (2.17 μm) and rat heart (1.78 μm; Fig. 4F). In a representative PEVK sequence of 821 amino acids from turtle heart connectin, both repeats of 26-28 amino acids and poly-E segments were present, which were also found in the N2BA isoform of mammalian heart connectin (Fig. 7D). The total frequency of

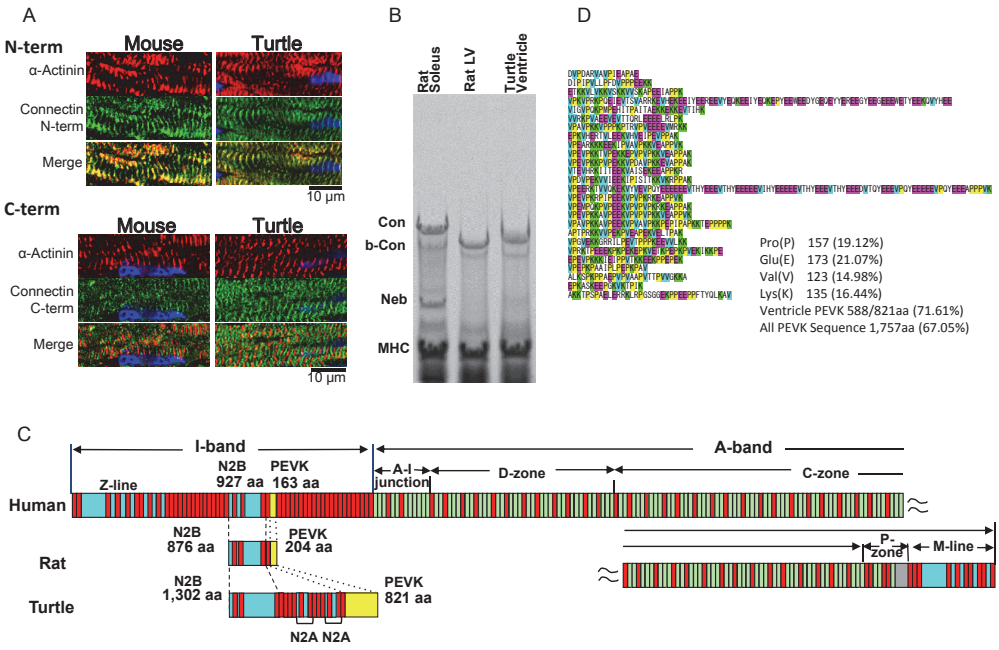

Fig. 7 Comparison of turtle heart connectin to mammalian heart connectin.
(A) Localization of connectin in turtle and rat ventricles. Turtle and rat ventricles were stained with N- or C-terminus connectin antibodies and α-actinin antibody and examined by fluorescence microscopy. Red, α-actinin antibody; green, connectin antibody.
(B) Molecular weights of connectin in turtle and rat ventricles. Whole extracts of turtle or rat ventricles were electrophoresed into SDS-Agarose gel. Whole extracts of rat soleus were also loaded as a molecular weight marker for high molecular weight proteins. Con, connectin; b-con, b-connectin; Neb, nebulin; MHC, myosin heavy chain.
(C) Domain structures of connectin in elastic region of turtle and rat ventricles. The regions amplified by RT-PCR are displayed with black lines and black numbers. Human, connectin form human ventricle. Rat, connectin form rat ventricle. Turtle, connectin form turtle ventricle. Red boxes, Ig domains; yellow box, PEVK domain; green boxes, Fn3 domains; light blue boxes, unique sequences. Dashed and dotted lines show N2B and PEVK domains, respectively.
(D) Amino acid sequence of a representative length of PEVK domain (P1, 821 amino acid) in turtle heart. Yellow: proline, pink: glutamate, blue: valine, green: lysine, aa: amino acids.

proline, glutamate, valine and lysine residues in the PEVK sequence from turtle heart connectin was 72%, which was similar to that in mammalian heart connectin (>70%).

DISCUSSION

We succeeded in characterizing the diastolic mechanical properties of both whole ventricles and isolated cardiomyocytes from turtle spongious ventricle and rat compact LV. Moreover, we showed that the lengths of elastic regions of connectin can be a molecular factor in affecting these mechanical properties. The major results that we obtained are: 1) a significantly larger chamber stiffness constant (b in $P = a \cdot e^{EDV \cdot b} + c$) obtained from normalized EDPVR in rat LV, representing their stiffer mechanical properties compared to turtle ventricles; 2) normalized EDPVRs obtained from turtle ventricles of varying weights spanned a relatively narrow range, indicating species-specific characteristics in ventricular compliance; 3) a significantly smaller decay constant of ventricular pressure (τ_L in $P(t) = \alpha / [1 + \exp(t/\tau_L)] + \beta$) in rat LV compared with turtle ventricle; 4) at the cellular level, the initial normalized stiffness of rat cardiomyocytes was 2.8 times higher than that of the turtle; and 5) the lengths of the elastic N2B and PEVK domains of connectin in turtle ventricles were larger than that in rat LV.

These results provide new insights regarding physiological differences in mechanical diastolic properties between turtle and rat ventricles i.e., ventricles consisting of a thick inner avascular spongious layer and those consisting of compact musculature that is only supplied by coronary vessels, respectively. Although many studies regarding anatomical and morphological differences in vertebrate hearts have been reported[24], investigations of mechanical functions of ventricles have been hampered by the difficulty in comparing functionality among variously sized and shaped hearts. In the present study, we demonstrated, for the first time, that the compact rat LV is much stiffer than the spongy turtle ventricle by a quantitative analysis of normalized EDPVRs. This suggests that mammalian ventricles have evolved to be stiffer because the ventricular chamber of turtles appears to represent an intermediate between amphibians, which are ancestral amniotes, and mammals[25].

The ventricles of turtles are in anatomical continuity, instead of being completely separated by a septum like the ventricles of mammals. It is well recognized that complete separation of the ventricles allows separate pulmonary and systemic circulation, which is critical for the energy-consuming endothermic lifestyle of mammals and aves[26, 27]. This evolutional change to the circulatory system required the morphological adaptation of myocardial architecture from spongy to compact musculature, which enabled a dual pressure system in the heart. Therefore, myocardial compaction throughout the ventricular wall is a significant event, which may independently have occurred in the evolution of mammals (synapsids) and birds (sauropsids)[26, 27].

In contrast to the restricted compliance, rat LV exhibited accelerated relaxation. Similarly, isolated rat cardiomyocytes showed a much shorter period from peak shortening to 50% relengthening and had a smaller time constant during relengthening compared with those of turtle cardiomyocytes. Rapid relaxation in the rat resulted in ventricular suction and early-phase filling (Fig. 3C). This may indicate that rat LVs possess restorative forces that generate sub-atmospheric pressure and result in a shorter isovolumic relaxation period and lower atrial pressure (Fig. 3B, C). In contrast, ventricles of turtles relaxed slowly and were mainly filled by atrial contraction during late-phase diastole. The greater contribution of atrial contraction accounts for the larger volume of the atrium in turtles (Fig. 3D). In mammals, atria reduced in size as the contribution of the atrium to ventricular filing lessened (Fig.

3E). As for Ca^{2+} handling, which plays a central role in myocardial contraction and relaxation, both the rates of increase and decrease of $[Ca^{2+}]_i$ were greater in rat cardiomyocytes than in turtle. One of the reasons for the rapid $[Ca^{2+}]_i$ dynamics in rat cardiomyocytes may be the T-tubules, which are tubular invaginations of the sarcolemma penetrating into the center of cardiomyocyte. These T-tubules accelerate the diffusion of Ca^{2+} to the myofibril and the sequestration of Ca^{2+} from the cytosol.

Although the primary structures of connectin in human, mouse[28, 29] and zebrafish[20] hearts has been reported, those in reptilian heart remained to be investigated. Here, for the first time, we determined the partial sequences of turtle heart connectin, including the elastic N2B and PEVK domains. Our results show that turtle ventricle exclusively expresses the larger N2BA isoforms of connectin, in contrast to human and rat hearts, which mainly express the smaller N2B isoform. Since the expression of N2BA isoforms is restricted to fetal and neonatal mammalian hearts, the expandability of turtle hearts may be similar to the expandability of neonatal mammalian hearts. In addition, turtle heart connectin contains two copies of the N2A region, which has never been observed in other vertebrate connectins, indicating that the original evolution of connectin occurred after the separation of turtles from the other reptiles 250 million years ago.

In turtle heart connectin, the length of N2B region (N2B exon) is 1,302 amino acids, which is larger than that of human (927 amino acids) and rat (876 amino acids). The PEVK sequence of turtle heart connectin was also determined, and its length is 821 amino acids, which is longer than in human (163 amino acids) and rat (204 amino acids). Because these elastic regions contributed to the extensibility of cardiomyocytes, the turtle heart was predicted to expand more easily than the mammalian heart. This prediction is entirely concordant with our extension experiments in cardiomyocytes.

It is important to examine the reason why mammalian ventricles evolved restricted compliance in order to obtain a better understanding of cardiac physiology. This study indicates that compact myocardium possesses stiffer diastolic mechanical properties, which closely relates to the blood supply by coronary circulation[8]. Coronary arterial flow, unlike that of other organs, is exclusively diastolic-dominant because intramyocardial vessels are squeezed by cardiac contraction, resulting in flow cessation[30]. Considering the stiff mechanical property in diastole and diastolic dominance of coronary arterial flow, we hypothesize that the compact myocardium of mammals became stiffer to preserve coronary arterial flow by preventing excessive ventricular expansion. This hypothesis can be applied to aves, the other vertebrate that possesses compact myocardium and well developed coronary circulation[8]. Further investigations are required to reveal the relation between ventricular stiffness and coronary circulation in vertebrate evolution among various species.

Clinically, heart failure with diastolic dysfunction occurs in more than 50% of all heart failure patients, and is considered to be more benign than systolic heart failure[31]. Possible therapeutic modalities to improve diastolic function have been reported. For example, inhibition of RNA binding Motif-20 a major connectin-splicing factor showed that upregulation of a compliant isoform of connectin improved diastolic function and exercise tolerance[32]. One possible interpretation of the high prevalence of diastolic heart failure in humans is that acquired impairment of diastolic function by cardiac hypertrophy or fibrosis with age tends to exceed the optimal range of ventricular diastolic mechanical stiffness. This is likely because cardiac function was strictly optimized for the reproductive years during cardiac evolution via an enhancement of relaxation and restriction of compliance.

This study has limitations. We did not evaluate diastolic function of the right ventricle (RV) in rats because EDPVRs obtained from excised hearts are greatly affected by the unphysiological deformation of septum. However, as an evaluation of a systemic pump that expels oxygenated blood to the body, normalized EDPVR is an appropriate concept because the stiffness constant of normalized EDPVR represents the stiffness per unit of myocardium. Therefore, physiological measures of stiffness constant are valuable, even if the volume ratio of blood flows toward pulmonary and systemic circuits is variable in turtles.

In conclusion, we investigated the diastolic function of turtle ventricles, consisting of spongious myocardium, and of rat compact LV. Turtle spongious ventricle possesses connectin with longer elastic regions (N2B and PEVK) than the connectin of rat LV, resulting in a more compliant mechanical property of isolated cardiomyocytes and ventricles compared with those of rat. These morphological and functional differences could be the results of evolutionary adaptation to the appearance of transmural coronary circulation, because the less compliant mechanical property of rat ventricle is largely advantageous to preserve diastolic-dominant coronary arterial flow by preventing excessive ventricular expansion when compared to the turtle's spongious ventricle without coronary circulation. Future basic research aimed at understanding the regulatory mechanism of the elasticity of cardiac connectin among broad vertebrates may contribute to accelerate the investigation of the therapeutic potential of diastolic heart failure.

ACKNOWLEDGEMENTS

This work was supported by JSPS KAKENHI Grant Number JP17H06272 and JP17H00859 to A.H., K.H., U.Y., and S.M., JP26282127 to K.H., U.Y., and S.M., JP26282127 to K.H., Y.U., and S.M., JP26702014 to Y.U. from the Ministry of Education, Culture, Sports, Science, and Technology of Japan, and was also supported by grants from Kawasaki Medical School. We thank Tomoko Yobimoto, Miki Sugino, and Aya Kodama for their invaluable technical assistance. We thank Prof. H. Miyazaki from Aino University for helping with preparation of reference glass microneedles to determine spring constants of the deflectable needles.

DISCLOSURES

There is no conflict of interest in this study.

REFERENCES

1) Borlaug BA, Kass DA: Mechanisms of diastolic dysfunction in heart failure. Trends Cardiovasc Med 16: 273-279, 2006

2) Jeong EM, Dudley SC Jr: Diastolic dysfunction. Circ J 79: 470-477, 2015

3) Ten Brinke EA, Burkhoff D, Klautz RJ, Tschöpe C, Schalij MJ, Bax JJ, van der Wall EE, Dion RA, Steendijk P: Single-beat estimation of the left ventricular end-diastolic pressure-volume relationship in patients with heart failure. Heart 96: 213-219, 2010

4) Angeja BG, Grossman W: Evaluation and management of diastolic heart failure. Circulation 107: 659-663, 2003

5) Ujihara Y, Iwasaki K, Takatsu S, Hashimoto K, Naruse K, Mohri S, Katanosaka Y: Induced NCX1 overexpression attenuates pressure overload-induced pathological cardiac remodelling. Cardiovasc Res 111: 348-361, 2016

6) Matsubara H, Takaki M, Yasuhara S, Araki J, Suga H: Logistic time constant of isovolumic relaxation pressure-time curve in the canine left ventricle. Better alternative to exponential time constant. Circulation 92: 2318-2326, 1995

7) Fukuda N, Granzier HL, Ishiwata S, Kurihara S: Physiological functions of the giant elastic protein titin in mammalian striated muscle. J Physiol Sci 58: 151-159, 2008

8) Oštádal B: Comparative Aspects of the Cardiac Blood Supply. Advances in Organ Biology 7: 91-110, 1999

9) Burkhoff D, Mirsky I, Suga H: Assessment of systolic and diastolic ventricular properties via pressure-volume analysis: a guide for clinical, translational, and basic researchers. Am J Physiol Heart Circ Physiol 289: H501-H512, 2005

10) Klotz S, Hay I, Dickstein ML, Yi GH, Wang J, Maurer MS, Kass DA, Burkhoff D: Single-beat estimation of

end-diastolic pressure-volume relationship: a novel method with potential for noninvasive application. Am J Physiol Heart Circ Physiol 291: H403-H412, 2006

11) Sagawa K, Maughan L, Suga H, Sunagawa K: Cardiac Contraction and the Pressure-Volume Relationship. New York, USA, Oxford University Press. 1988, pp156-159

12) Suga H: Ventricular energetics. Physiol Rev 70: 247-277, 1990

13) Katanosaka Y, Iwasaki K, Ujihara Y, *et al.*: TRPV2 is critical for the maintenance of cardiac structure and function in mice. Nat Commun 5: 3932, 2014

14) Prosser BL, Ward CW, Lederer WJ: X-ROS signaling: rapid mechano-chemo transduction in heart. Science 333: 1440-1445, 2011

15) Pasqualin C, Gannier F, Yu A, Malécot CO, Bredeloux P, Maupoil V: SarcOptiM for ImageJ: high-frequency online sarcomere length computing on stimulated cardiomyocytes. Am J Physiol Cell Physiol 311: C277-C283, 2016

16) Kishino A, Yanagida T: Force measurements by micromanipulation of a single actin filament by glass needles. Nature 334: 74-76, 1988

17) Miyazaki H, Hasegawa Y, Hayashi K: A newly designed tensile tester for cells and its application to fibroblasts. J Biomech 33: 97-104, 2000

18) Nishimura S, Yasuda S, Katoh M, Yamada KP, Yamashita H, Saeki Y, Sunagawa K, Nagai R, Hisada T, Sugiura S: Single cell mechanics of rat cardiomyocytes under isometric, unloaded, and physiologically loaded conditions. Am J Physiol Heart Circ Physiol 287: H196-H202, 2004

19) Galli GL, Taylor EW, Shiels HA: Calcium flux in turtle ventricular myocytes. Am J Physiol Regul Integr Comp Physiol 291: R1781-R1789, 2006

20) Hanashima A, Hashimoto K, Ujihara Y, Honda T, Yobimoto T, Kodama A, Mohri S: Complete primary structure of the I-band region of connectin at which mechanical property is modulated in zebrafish heart and skeletal muscle. Gene 596: 19-26, 2017

21) Yajima H, Ohtsuka H, Kume H, Endo T, Maruyama K, Kimura S, Maruyama K: Molecular cloning of a partial cDNA clone encoding the C terminal region of chicken breast muscle connectin. Zoolog Sci 13: 119-123, 1996

22) Soeno Y, Yajima H, Kawamura Y, Kimura S, Maruyama K, Obinata T: Organization of connectin/titin filaments in sarcomeres of differentiating chicken skeletal muscle cells. Mol Cell Biochem 190: 125-131, 1999

23) Warren CM, Krzesinski PR, Greaser ML: Vertical agarose gel electrophoresis and electroblotting of high-molecular-weight proteins. Electrophoresis 24: 1695-1702, 2003

24) Victor S, Nayak VM, Rajasingh R: Evolution of the ventricles. Tex Heart Inst J 26: 168-175, 1999

25) Webb GJ, Heatwole H, de Bavay J: Comparative cardiac anatomy of the reptilia. II. A critique of the literature on the Squamata and Rhynchocephalia. J Morphol 142: 1-20, 1974

26) Farmer CG: Evolution of the vertebrate cardio-pulmonary system. Annu Rev Physiol 61: 573-592, 1999

27) Koshiba-Takeuchi K, Mori AD, Kaynak BL, *et al.*: Reptilian heart development and the molecular basis of cardiac chamber evolution. Nature 461: 95-98, 2009

28) Labeit S, Kolmerer B: Titins: giant proteins in charge of muscle ultrastructure and elasticity. Science 270: 293-296, 1995

29) Granzier H, Radke M, Royal J, Wu Y, Irving TC, Gotthardt M, Labeit S: Functional genomics of chicken, mouse, and human titin supports splice diversity as an important mechanism for regulating biomechanics of striated muscle. Am J Physiol Regul Integr Comp Physiol 293: R557-R567, 2007

30) Kajiya F, Zamir M, Carlier S: Cardiac hemodynamics, coronary circulation and interventional cardiology. Ann Biomed Eng 33: 1728-1734, 2005

31) Abhayaratna WP, Marwick TH, Smith WT, Becker NG: Characteristics of left ventricular diastolic dysfunction in the community: an echocardiographic survey. Heart 92: 1259-1264, 2006

32) Methawasin M, Strom JG, Slater RE, Fernandez V, Saripalli C, Granzier H: Experimentally Increasing the Compliance of Titin Through RNA Binding Motif-20 (RBM20) Inhibition Improves Diastolic Function In a Mouse Model of Heart Failure With Preserved Ejection Fraction. Circulation 134: 1085-1099, 2016